Application of an Auxiliary Wheel Cleaning System in the Grinding of SPK Tool Steel

hamed adibi (hadibi@aut.ac.ir)
Amirkabir University of Technology https://orcid.org/0000-0002-9956-0344
Omid Hatami
Amirkabir University of Technology
Seyed Mehdi Rezaei
Amirkabir University of Technology

Research Article

Keywords: Grinding, wheel loading, wheel cleaning, coolant, image process

Posted Date: February 19th, 2021

DOI: https://doi.org/10.21203/rs.3.rs-216941/v1

Abstract

Grinding operation is one of the most complex and accurate machining processes whose performance is highly dependent on the surface conditions of the grinding wheel. As the friction between abrasive grains and the workpiece results in a large amount of heat, the use of coolant can prevent the workpiece surface from burning, microstructure alteration, subsurface damages, and hardness variation. To get better the cleaning of the abrasive grains on the surface of the wheel during the grinding process, this paper is focused on the performance of an auxiliary compressed air jet system during grinding of hard-to-grind materials. Moreover, the wheel loading of the grinding wheel will also be evaluated. Different incident angles of the compressed air nozzle (0˚, 30˚, 45˚, and 60˚) were examined. Furthermore, conventional flood coolant, as well as drying with and without a cleaning system, was applied for comparison purposes. Surface roughness, tangential forces, specific energy, wheel loading analysis, and SEM images were evaluated where the incident angle of 45˚ led to the best results. Wheel loading resulted in the accumulation of chips between abrasive grains to the top of cutting grains. Detection and identification of loading has been operated based on image processing technique.

1. Introduction

Grinding refers to machining with high-speed abrasive wheels. A wide variety of sizes and types of abrasives are used in this technique [1]. This process requires a substantial amount of power to shear one unit of removal material. Thus, a combination of a countless number of cutting edges as abrasive grains will result in significant energy consumption which will dissipate as heat on the cutting zone. The generated heat upon the interaction of the work piece and grinding wheel is the major reason for the damage of the workpiece, it also shortens the life of the grinding wheel [2, 3]. Multiple sharp edges of the abrasive grains deform and shear the surface of the workpiece [4][16]. The excessive increase of machining temperature and the intensification of the grinding wheel loading are the significant repercussions of this technique. Hot chips and particles produced in grinding have an affinity to fill the pores of the wheel if they are not completely removed from the cutting zone. When these particles lodge in the pores of grinding wheel, they impair the effect of the coolant in the cutting zone and further disturb the cooling and lubrication of the grinding zone [5, 6].

Several studies have been conducted not only to understand the origin of the wheel loading phenomenon but also to investigate the wheel loading under different parameters (wheel speed, cutting depth, and feed rate) [7]. If chips fill inside the pores of the wheel as the grinding process continues, it will harmfully affect dimensional and geometrical quality. Additionally, this will require more frequent dressing at short intervals [8].

Upon the enhancement of the tangential forces, the grinding wheel needs to be sharpened by special techniques depending on the type of grinding wheel. With an increase in sharpening, the grinding wheel lifetime will be decreased, especially in the case of super-abrasive grinding wheels [9].

A cutting-edge manner to reduce the wheel loading phenomenon maintains high-porosity grains on the wheel surface and opens the wheel structure by a constant dressing. However, this will result in high wheel costs [10]. It has been revealed that the use of a second nozzle based on wheel cleaning can significantly enhance grinding performance [10] [11]. Along with cleaning the nozzle, cutting fluids could be applied to the cutting zone. Cutting fluids have three significant functions; lubrication of the contact area between the workpiece and grinding wheel, chips cleaning and keeping them away from the cutting zone, and cooling the workpiece [12]. Moreover, an innovative method has been developed based on cooled air and cleaning jet to resolve the problems caused by temperature and clogging in the cutting zone [2, 13].

Application of a compressed air jet under different angles as an auxiliary nozzle can improve the wheel cleaning [13, 14]. In this research, the effectiveness of such technology will be evaluated and the effectiveness of the air jet direction and its pressure in removing the adhered particles from the wheel surface will be studied. Four auxiliary wheel cleaning nozzles including 0°, 30°, 60°and 90° were used to remove chips from the grinding zone. Tangential air jet might only little doing between the abrasives and adhered particles. Their adhesion could be contributed by air jets with an inclination angle of 60° as well as 90° which could directly push the chips toward the abrasive layers and pores of the wheel. Forcing the chips off the grinding surface could be achieved with the optimum inclination angle of 30° which enables the air to penetrate the interface between the wheel surface and chips.

Regarding the importance of detecting and identifying wheel loading, a method was developed based on image processing by Matlab to detect wheel loading on the grinding wheel as well as evaluating its percentage [15, 16]. The main advantage of image processing is its high speed as well as low cost. It takes roughly 0.4 s to process a picture [10].

2. Experimental Procedure

The grinding machine used in these tests is BLOHM Surface Grinder (model HFS204). It was equipped with a vitrified bond grinding wheel 32A46 JVBE 268445 manufactured by NORTON. All the input parameters are shown in *Table.1.*

The dynamometer is made by KISTLER Company in Germany (model 92558). The applied workpiece is a brittle-hard SPK tool steel with DIN1.2080 standard which is widely-used steel. Tool steel contains 2.1% carbon as well as 12% Chromium. To reduce the hardness and stress of the workpiece, it was hardened and tempered before the grinding process.

Figure.1 schematically depicts the setup. Several incident angles of the cleaning nozzle, , were tested (0°, 30°, 45°, and 60°). The cleaning nozzle is an adjustable device whose angle could be altered, in this essay, however, only the mentioned angles were taken into account.

For a better understanding of the efficiency of different cleaning systems compared to the application of flood coolant and Dry without cleaning, the surface roughness of the workpiece was measured and its

average value was used for the analysis. Average roughness was measured by using Marsurf XR 1 surface roughness tester. Output Roughness parameters were Ra, Rz, Rq, Rp.

Ra is the arithmetic average of the absolute values of the profile heights over the evaluation length which were set to 4mm. Rp is the peak height and Rz stands for the vertical distance between the peak and deepest points of the surface. Rq also denotes the root mean square average of the profile heights over the assessed distance [17].

The three-dimensional ground surface was obtained using Profilometer as shown in *Figure.2.a* obtained using Leitz WETZLAR microscope with 250x magnification. *Figure 2.b* also shows the image from the surface of the grinding wheel taken by optical microscopy. *Figure 2.c* depicts Scanning electron microscopy (SEM) images to observe ground surface and chips in all conditions.

3. Results And Discussion

3.1. Surface roughness

*Figure.3.*shows the surface roughness parameters of the tool steel workpiece under various cooling and cleaning conditions. Input parameters such as grinding wheel speed (20 m/s), cutting depth (20μm) and feed rate (100 mm/s) were kept constant. Cutting fluids were used with and without a cleaning system at different incident angles. The samples were ground at 8 passes with a constant depth of cut and after the grinding process, surface roughness tests were performed by the roughness tester. When the compressed air cleaning nozzle jet was employed to clean the wheel, parameters of surface roughness values decreased. The worse quality of workpiece was observed in the process of coolant without cleaning which can be assigned to chips lodging the wheel pores and abrasive layers. Roughness parameters improved at the incident angle of 30°. In the incident angle of 0°, the cleaning nozzle was tangential to the horizontal axis, helping the chips get entangled on the surface of the grinding wheel instead of cleaning the wheel. Having a clogged wheel surface, even though the ground surface will have better surface roughness for a short time, surface and subsurface damages are expected if the grinding continues for a long time. As the cleaning nozzle helps to remove chips off the wheel surface, the number of active abrasive grains with sharp cutting edges on the surface of the wheel increases. Even though this helps reducing grinding force, but it also helps increasing surface roughness. This is shown at the incident angle of 45°.

The values of surface parameters were evaluated over 0.8 mm. It is recommended to assess these parameters at five sampling lengths. Here, it was adjusted at 5 sampling lengths.

Figure.4 depicts the surface roughness profile of the workpiece ground using coolant without a cleaning system. It presented a higher range of peaks and valleys, leading to higher average arithmetic roughness values, as a result; more scratches occurred on the surface of the workpiece, giving rise to poor surface roughness. *Figure.5* shows the surface roughness profile of the sample ground by coolant along with a cleaning system under the incident angle of 0°. It exhibited great results, compared to the 30° and 45°

incident angles. Based on tangential forces, the fine finishing surface of 0° could be attributed to the chips clogged on the pores of the corresponding wheel surface leading to the engagement of most of the flatted abrasive grains with the workpiece. However, this will help in achieving a fine surface for a short time. *Figure 6 and Figure 7* show surface roughness under the incident angle of 30° and 45°, respectively. As the inclination angle increased, the ability of the compressed air jet to remove the clogged chips was enhanced. The increased roughness values could be attributed to the diminishing the distance of abrasive grains on the wheel surface as the nozzle helps to remove chips and reveal most of the grains.

In the optimum conditions of wheel cleaning parameters, surface roughness values were lesser than 0.6 Ra (μm), which is usually a limit value for grinding operations. However, the surface roughness of coolant with the cleaning system under the incident value of 0° was lower than 0.4 Ra (μm), which is a great result for grinding operation. It can be, however, attributed to the chips lodged on the surface of the grinding wheel which will culminate in less surface roughness. However, surface and subsurface damages as well as burning significantly grew in a clogged wheel.

As the depth of cut, feed rate, and cutting speed increased, the surface roughness incremented as well. By reducing the grinding depth of cut in tool steel with alumina grinding wheel, most of the energy will be spent on rubbing and plowing, thus, less energy will contribute to the chip formation. Additionally, this is the reason for the deterioration of the surface roughness with the increase in depth of cut. Cutting fluid also plays a decisive role in forcing chips off the grinding zone, besides, it minimizes the temperature of the cutting region, hence leading to fine surface finishing [8, 13].

3.2. Tangential force

Figure 8 presents the tangential force of tool steel workpiece under different cooling conditions and cleaning systems. Input parameters such as cutting speed (20 m/s), depth of cut (20 μm), and feed rate (100 mm/s) were kept constant throughout the experiments.

Comparing cutting forces in the state of Dry and coolant with and without using a cleaning system, the cutting forces should have less tangential cutting forces due to the cooling of the grinding wheel in the state of coolant. In the horizontal position and nozzle angle of 30°, the situation was worsened. This can be attributed to the chips clogged on the surface of the wheel which cannot be removed by the cleaning nozzle [18]. In these two cases, the air nozzle helps the chips to adhere and get stuck on the pores of the grinding wheel, increasing both loading and forces [19]. The best performance of the cleaning system was observed at the angle of 45°, where the grinding forces were reduced in both dry and cooled states. In these two cleaning systems, the wheel maintained its sharpness longer, producing less tangential force. At the incident angle of 45°, the cleaning systems broke up the air barrier due to wheel rotation. This forced the chips off the wheel surface and finally led to lower wheel loading [13] [8].

3.3. Specific energy

The specific grinding energy of the tool steel workpiece is depicted in *Figure.9* under different cooling and cleaning conditions where cutting speed (20 m/s), depth of cut (20 μm), and feed rate (100 mm/s) were maintained at constant values. Cooling and the use of a satisfactory cleaning system at the incident angle of 45° declined the friction force between the abrasive grains and the workpiece, resulting in reduced grinding forces and specific grinding energy. Moreover, not only adequate cooling in grinding reduced the specific energy but it also improved the surface quality and dimensional accuracy. Based on Equation (2), the tangential cutting force (F_t) and speed of the grinding wheel (V_c) are directly related to the specific energy [5]. The best performance in dry and coolant state was achieved at the nozzle angle of 45°. Equation (4) was used to evaluate the volumetric material removal, where, *d* is the depth of cut, *b* shows the width of the wheel, *L* denotes the longitudinal distance of grinding and *N* is the number of grinding passes.

$$U = \frac{p}{Ow} \tag{1}$$

$$p = F_t.V_c \tag{2}$$

$$Q_w = d.b.V_w \tag{3}$$

$$Z_w = d.b.L.N \tag{4}$$

The following image processing techniques will demonstrate how to use image normalization, edge detection, image segmentation, and morphological operations to identify wheel loading.

3.4. Image analysis

To investigate the topographic details of the SPK tool steel, 1.4 mm 1.4mm of ground surface area was three-dimensionally analyzed using profilometry as shown in *Figure.10.a*. The Boltzmann Bent Step curves were then plotted from three-dimensional profiles with the help of Gwydion software coupled with the profilometer [20]. As shown in *Figure.10, the* 3-D profile of the dry state without the cleaning system led to the worst surface roughness with deepest grooves. The difference between the deepest valley and the peak was 180μm. In *Figure.10.b,* the surface topology is shown from 0.03mm to 0.130 mm. The height distribution provides information about the percentage of valleys and peaks*. Figure.11* shows the 3-D profile of dry state with cleaning which exhibited less surface roughness compared to the previous case. Employing both cutting fluids and wheel cleaning led to the smallest grooves as shown in *Figure.12*, which exhibits a 3-D profile, representing a plateaued model of the surface. The red curve

shows the Boltzmann Bent Step along the ground surface, which indicates a peaky surface when the surface of the workpiece was plastically deformed. The plateaued type of surface can be also observed on the two edges of the curve [20].

Figure 14.a shows the SEM images of the ground surface. Aside from the severe plastic deformation caused by abrasive grains and clogged chips on the wheel surface, material removal was irregular and inefficient. Material redisposition and smearing were the main causes of the surface burning which is obvious with white edges as shown in *Figure14.b*. When the cutting fluids failed to flush and clean the cutting zone, it damaged the ground surface and subsurface, giving rise to grooves and narrow furrows. Clogged chips tend to increase rubbing and plowing on the ground surface, resulting in poor surface roughness. To get a deeper understanding of the surface topography of the ground workpiece, the three-dimensional profile of the corresponding ground surface was observed. As suggested in *Figure.14.c,* the middle of the surface experience severe plastic deformation.

Figure.15.a.b shows the workpiece ground by cutting fluids along with a cleaning system at 45°. The fine finishing surface of the workpiece can be attributed to the application of the cleaning nozzle as well as cutting fluid. A better way to diminish the impact of produced heat on the workpiece is using cutting fluids, which results in a fine finishing surface. Three-dimensional profile exhibits the peaks and valleys of surface, which shows fine finishing surface due to the use of both cutting fluids and cleaning nozzle, which helped in breaking up the air barrier around the wheel.

Image processing technique

The performance of the image processing technique can be divided into the following four steps: image normalization, edge detection, image segmentation, and morphological operations [10, 21]. In these steps, instructions are applied to examine the image processing and apply different filters to separate and detect the loading of the grinding wheel (see *Figure 16*).

Wheel loading

Abrasive grains on the grinding wheel are in contact with the surface of the workpiece and act as a cutting tool to produce chips. The surface of the grinding wheel always contains irregularities or free spaces. Real contact only occurs on some cutting edges that are taller than the other grains [22]. This deforms the workpiece and causes intermetallic adhesion in the contact zone, resulting in cold welding contacts between the abrasive grains and the removed chips. The loading mechanism can be described by the separated chips during grinding which lodge to the free spaces between abrasive grains and bond on the wheel surface [7, 10].

Figure.17.a presents the surface of the grinding wheel after grinding taken by optical microscope under the magnification of 250x. Sharp reflected particles are loadings on the wheel surface, which have high

intensity. In *Figure 17.b*, the 3-D topography of the previous picture is processed by Gwyddion. If such a grinding wheel is employed in the grinding zone, it will scratch the workpiece surface, thus raising the surface roughness. Red areas show the loading on the surface of the wheel while the pale red areas are indicative of active abrasive grains involving in the cutting process.

Figure 18.a exhibits the wheel clogging phenomenon. The picture was taken from the ground surface under the magnification of 250x using an optical microscope. It could be seen from the picture the clogged chip suffered severe plastic deformation, furthermore, it was rubbed against the workpiece causing rubbing as well as plowing. *Figure 18.b* shows the protrusion of point A to B which is more exposed to the other places. Additionally, resistance to grain dislodgment in this region can be maintained due to the anchoring of the grains provided by the clogged material. The ground workpiece showed higher surface roughness. This irregularity of grain distribution can be prevented by the protrusion which is produced by the chips clogged in the wheel pores.

Figure.19 exhibits the effect of a compressed air jet nozzle in the cleaning wheel surface. The middle of the wheel which was exposed to the air nozzle showed the least amount of loading. The nozzle angle of 45° led to the best results in terms of cleaning the surface from loading and chips. Detection of loading is complicated and can be a time-consuming and expensive process. A novel technique is presented here based on the image processing process using the Matlab toolbox to detect the loadings. The main advantage of this method is its fast performance and lower costs. The image processing time is 0.4 seconds and it only takes 5 seconds to process the entire image taken from the grinding wheel. It starts with an optical microscope to capture images from the surface of the grinding wheel after each grinding pass. Forty images were taken to obtain a loading across the grinding wheel. After the surface morphology step, the number of white pixels was divided by the total number of white and black pixels to obtain the grinding wheel loading. The optical properties of metal chips, abrasive grains, and wheel loading have been considered. Experiments were also performed to evaluate the repetition of the proposed technique.

Figure.20 shows the amount of loading of the grinding wheel relative to the total volumetric material removal of the SPK tool steel workpiece in the dry state using the alumina grinding wheel with and without cleaning system at the nozzle angle of 45°. In this experiment, input parameters such as grinding wheel speed (20m/s), depth of cut (20 μm), feed rate (100 mm/s), and incident angle of the nozzle were kept constant. After each experiment, the surface of the grinding wheel was imaged using an optical microscope to process the average loading of the grinding wheel surface using MATLAB. As the grinding process began, chips were stuck in the free space between the abrasive grain and the grinding wheel bond, increasing the friction between the abrasive grains and surface of the workpiece in the cutting zone, thus, enhancing the grinding force. When the wheel loading over the surface of the wheel approached the saturated state, the movement between the wheel and workpiece changes to sliding friction, as a consequence, most of the grains cannot tolerate the excessive grinding force and friction, as a result, they tend to fall off the grinding wheel. This will alter the morphology and topology of the wheel surface.

Moreover, self-sharpening of the abrasive grains may occur under a continuous grinding process. Finally, fewer grinding forces and lower temperatures will be achieved.

Dry grinding state with cleaning system under the incident angle of 45° showed the lowest loading (63.39%), compared to dry state without cleaning system.

Figure.21 presents the amount of loading in the grinding wheel relative to its volumetric material removal from SPK tool steel workpiece with alumina grinding wheel in coolant state with and without cleaning system. In the case of using the cutting fluid, many chips were separated from the grinding zone with help of cutting fluids, giving rise to less wheel loading in the coolant state compared to the Dry case [10]. Conventional cutting fluid state with cleaning system under the incident angle of 45° showed the lowest loading (38.58%), compared to coolant state without cleaning system.

Figure.22 indicates the changes in the incident angle of the cleaning nozzle system along with the specific grinding energy against the volumetric material removal in the tool steel workpiece. At the incident angle of 0 ˚, the adhesion of the chips to the pores of the grinding wheel was intensified. The nozzle of the cleaning system indeed assisted chips to adhere to the surface of the grinding wheel. At the incident angle of 60 ˚, the cleaning jet did not help to reduce the loading at all. At the incident angle of 30 ˚, only a part of the loading from the surface of the grinding wheel was removed. But at the incident angle of 45 ˚, the least amount of wheel loading as well as specific energy was observed [10]. A decrease in wheel loading at an angle of 45° declined the friction, cutting, and specific forces.

Wheel loading with changing the depth of cut, cutting speed, and feed rate.

Figure.23, shows the loading of grinding wheels at different depths of cut (20, 40, and 60 μm) against the volumetric material removal. As seen, the least amount of wheel loading can be achieved at the depth of cut of 20 μm. With an increase in depth of cut and thereby an enhancement in interactions between abrasive grains and workpiece, many active cutting grains will take part in material removal. A higher depth of cut will lead to a greater removal rate due to longer grit grinding length and higher temperature, thereby causing more severe wheel loading [23]. *Figure.24* shows the results with increasing the cutting speed. The best performance was achieved at the speed of 20m/s which also led to lower wheel loading. Since increasing cutting speed leads to a decrease in the cutting force, it will also increase in several grinding passes. *Figure.26* exhibits the results of increasing feed rate. A decrease in average force per grain could be detected with a decline in the feed rate. At a higher feed rate, the average force per grain tended to higher values. To increase the volumetric material removal, it is recommended to enhance the feed rate rather than the depth of cut [7].

Conclusion

This paper addressed the grinding of SPK tool steel under different cooling and cleaning methods. The main conclusions can be listed as follows:

- The surface roughness decreased by 30.91% while using the wheel cleaning system along with coolant under the incident angle of 0˚ as compared with coolant state without cleaning. Under the incident angle of 30˚ and 45˚, roughness percentage values decreased by 11.60 and 2.29%, respectively. If the grinding wheel contains sharp grain edges, this will result in a rough surface and lower tangential forces. Moreover, for clogged wheels, roughness parameters decremented. At the incident angle of 30˚ and 45˚, roughness values approached the values obtained under the use of coolant without cleaning. Furthermore, an increment in the depth of cut enhanced the cutting speed, feed rate, and roughness.
- Based on the results from tangential forces and specific energy in different cleaning and cooling system, in the state of coolant and Dry with cleaning system under the incident angle of 45˚, tangential forces and specific energy decreased by 35.59 and 26.15% as compared to Dry and Coolant without cleaning, respectively. This could be attributed to the sharp cutting edges of abrasive grains.
- The highest cleaning effect, as well as the lowest amount of loading of the grinding wheel, occurred at the nozzle angle of 45 along with dry and coolant state. Compared to the dry and cooling state without cleaning, it reduced the wheel loading by 63.39 and 38.58%, respectively.
- The best performance of wheel cleaning and specific energy was obtained at the incident angle of 45˚. Moreover, SEM images of the ground surface with and without using coolant at 45˚ were taken which showed a quite fine finishing in the surface ground using coolant and cleaning system operating at the nozzle angle of 45˚.
- The wheel loading, surface roughness, and grinding forces increased with enhancing the depth of cut, feed rate, and cutting speed.

Declarations

Funding

No funding was received to assist with the preparation of this manuscript.

Conflicts of interest/Competing interests

The authors declare that they have no competing interests.

Availability of data and material

Not applicable.

Ethics approval

Not applicable.

Consent to participate

Not applicable.

Consent for publication

Not applicable.

Authors' contributions:

Hamed Adibi: supervision, investigation, providing resources and equipment, project administration.

Omid hatami: investigation, performing experimental analysis, performing numerical simulations,

Seyed mehdi rezaei: supervision, investigation, providing resources and equipment, project administration.

References

1. Chen, J., et al., *Theoretical study on brittle–ductile transition behavior in elliptical ultrasonic assisted grinding of hard brittle materials.* Precision Engineering, 2016. **46**: p. 104-117.
2. Yanase, Y., M. Komori, and M. Ochi, *Grinding of internal gears by setting a large crossed-axes angle using a barrel-shaped grinding wheel.* Precision Engineering, 2018. **52**: p. 384-391.
3. Alagumurthi, N., K. Palaniradja, and V. Soundararajan, *Heat generation and heat transfer in cylindrical grinding process-a numerical study.* The International Journal of Advanced Manufacturing Technology, 2007. **34**(5-6): p. 474-482.
4. Guo, B. and Q. Zhao, *Ultrasonic vibration assisted grinding of hard and brittle linear micro-structured surfaces.* Precision Engineering, 2017. **48**: p. 98-106.
5. de Jesus Oliveira, D., et al., *Improving minimum quantity lubrication in CBN grinding using compressed air wheel cleaning.* Journal of Materials Processing Technology, 2012. **212**(12): p. 2559-2568.
6. Rodriguez, R.L., et al., *Evaluation of grinding process using simultaneously MQL technique and cleaning jet on grinding wheel surface.* Journal of Materials Processing Technology, 2019. **271**: p. 357-367.
7. Agarwal, S., *On the mechanism and mechanics of wheel loading in grinding.* Journal of Manufacturing Processes, 2019. **41**: p. 36-47.
8. Bianchi, E.C., et al., *Application of the auxiliary wheel cleaning jet in the plunge cylindrical grinding with minimum quantity lubrication technique under various flow rates.* Proceedings of the Institution of Mechanical Engineers, Part B: Journal of Engineering Manufacture, 2019. **233**(4): p. 1144-1156.

9. Cameron, A., R. Bauer, and A. Warkentin, *An investigation of the effects of wheel-cleaning parameters in creep-feed grinding.* International Journal of Machine Tools and Manufacture, 2010. **50**(1): p. 126-130.
10. Adibi, H., S. Rezaei, and A.A. Sarhan, *Grinding wheel loading evaluation using digital image processing.* Journal of Manufacturing Science and Engineering, 2014. **136**(1).
11. Adibi, H., S. Rezaei, and A.A. Sarhan, *Investigation on using high-pressure fluid jet in grinding process for less wheel loaded areas.* The International Journal of Advanced Manufacturing Technology, 2014. **70**(9-12): p. 2233-2240.
12. de Souza Ruzzi, R., et al., *MQL with water in cylindrical plunge grinding of hardened steels using CBN wheels, with and without wheel cleaning by compressed air.* The International Journal of Advanced Manufacturing Technology, 2017. **90**(1-4): p. 329-338.
13. Lopes, J.C., et al., *Grinding performance using variants of the MQL technique: MQL with cooled air and MQL simultaneous to the wheel cleaning jet.* The International Journal of Advanced Manufacturing Technology, 2019. **105**(10): p. 4429-4442.
14. Garcia, M.V., et al., *Grinding performance of bearing steel using MQL under different dilutions and wheel cleaning for green manufacture.* Journal of Cleaner Production, 2020. **257**: p. 120376.
15. Feng, Z. and X. Chen, *Image processing of the grinding wheel surface.* The International Journal of Advanced Manufacturing Technology, 2007. **32**(5-6): p. 452-458.
16. Adibi, H., S. Rezaei, and A.A. Sarhan, *Analytical modeling of grinding wheel loading phenomena.* The International Journal of Advanced Manufacturing Technology, 2013. **68**(1-4): p. 473-485.
17. Hommel, A., *Surface Roughness Terminology and Parameters.* CT, USA: New Britain, 1988.
18. Lopes, J.C., et al., *Application of a wheel cleaning system during grinding of alumina with minimum quantity lubrication.* The International Journal of Advanced Manufacturing Technology, 2019. **102**(1-4): p. 333-341.
19. Bianchi, E.C., et al., *Plunge cylindrical grinding with the minimum quantity lubrication coolant technique assisted with wheel cleaning system.* The International Journal of Advanced Manufacturing Technology, 2018. **95**(5-8): p. 2907-2916.
20. Choudhary, A., A. Naskar, and S. Paul, *Effect of minimum quantity lubrication on surface integrity in high-speed grinding of sintered alumina using single layer diamond grinding wheel.* Ceramics International, 2018. **44**(14): p. 17013-17021.
21. Gonzalez, R.C., R.E. Woods, and S.L. Eddins, *Digital image processing using MATLAB*. 2004: Pearson Education India.
22. Liu, C.-S. and Y.-A. Li, *Evaluation of grinding wheel loading phenomena by using acoustic emission signals.* The International Journal of Advanced Manufacturing Technology, 2018. **99**(5-8): p. 1109-1117.
23. Gu, Y., et al., *Towards the understanding of creep-feed deep grinding of DD6 nickel-based single-crystal superalloy.* The International Journal of Advanced Manufacturing Technology, 2019. **100**(1-4): p. 445-455.

Tables

Table1 . Grinding condition

Grinding model	BOHLEM Surface Grinder with model HFS204
Grinding wheel	White Alumina- 32A46 JVBE 268445
Dynamometer	KISTLER company with 92558 model
Cutting speed (-m/s)	15; 20; 25; 30
Feed rate (mm/s)	100; 300; 500
Depth of cut(µm)	20; 40; 60
Conventional cutting fluid	Semi-synthetic vegetable oil based emulsion
Flow rate for conventional technique	17 (l/min)
Air pressure in cleaning system (MPa)	0.6 MPa
Workpiece material	hardened and tempered tool steel (SPK)
Cooling/cleaning methods	Flood coolant Dry Air jet with angle of 0˚ Air jet with angle of 30˚ Air jet with angle of 45˚ Air jet with angle of 60˚
Dresser	Diamond single point
Dressing depth (µm)	50 µm in 2 passes
Dressing speed (mm/min)	100
Sparkout (second)	8 sec

Figures

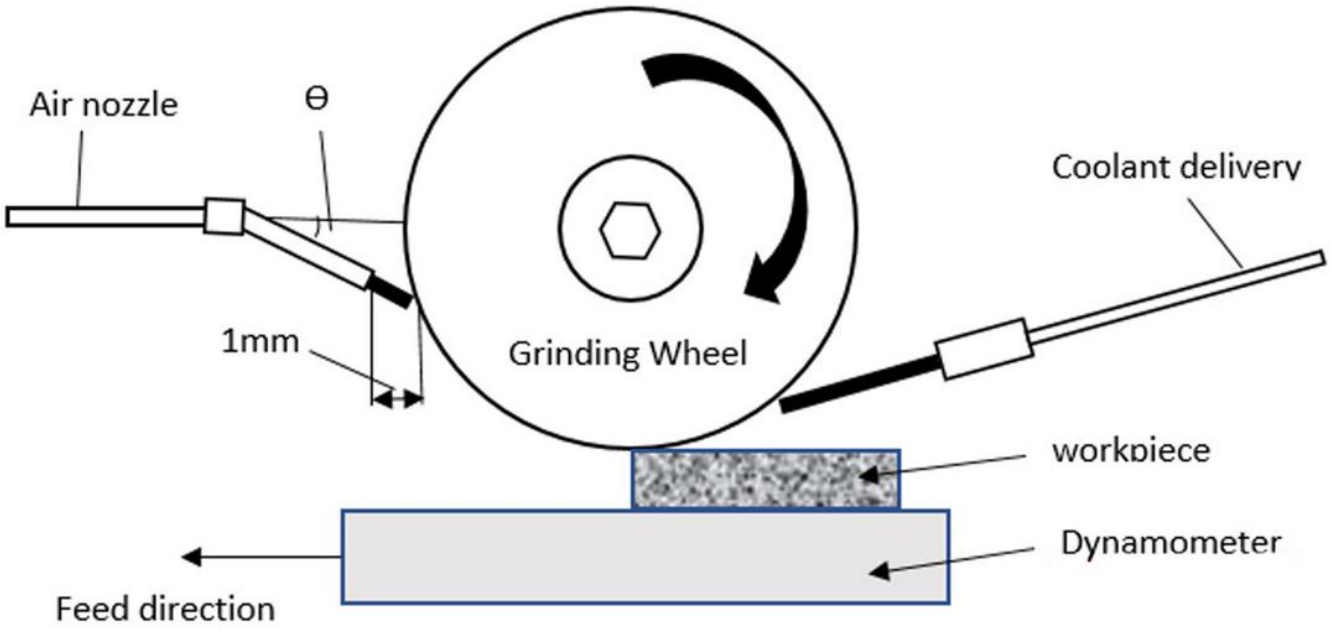

Figure 1

Schematic of the setup.

a) profilometer *b) light microscopy* *c) SEM*

Figure 2

instruments used to capture images

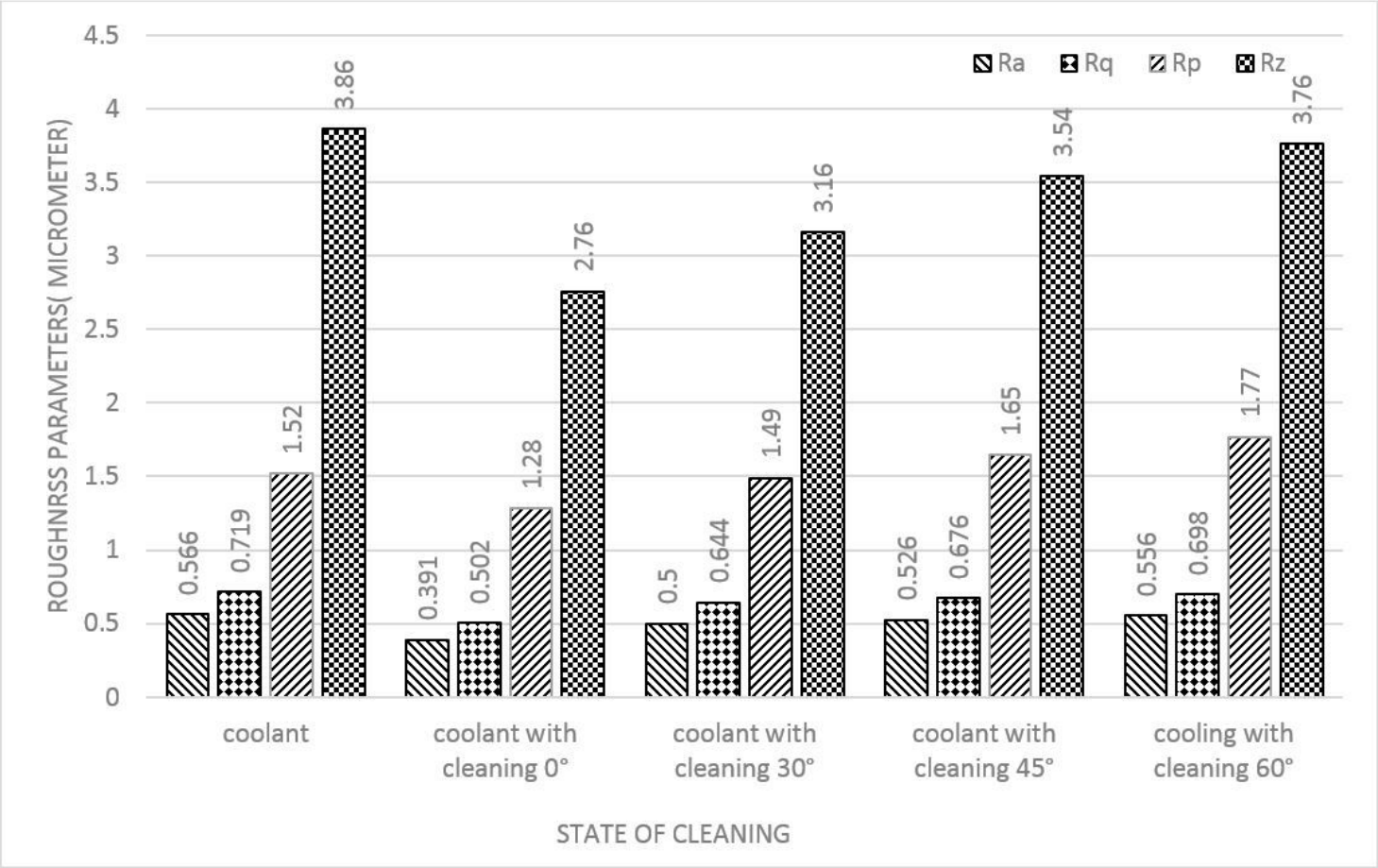

Figure 3

surface roughness

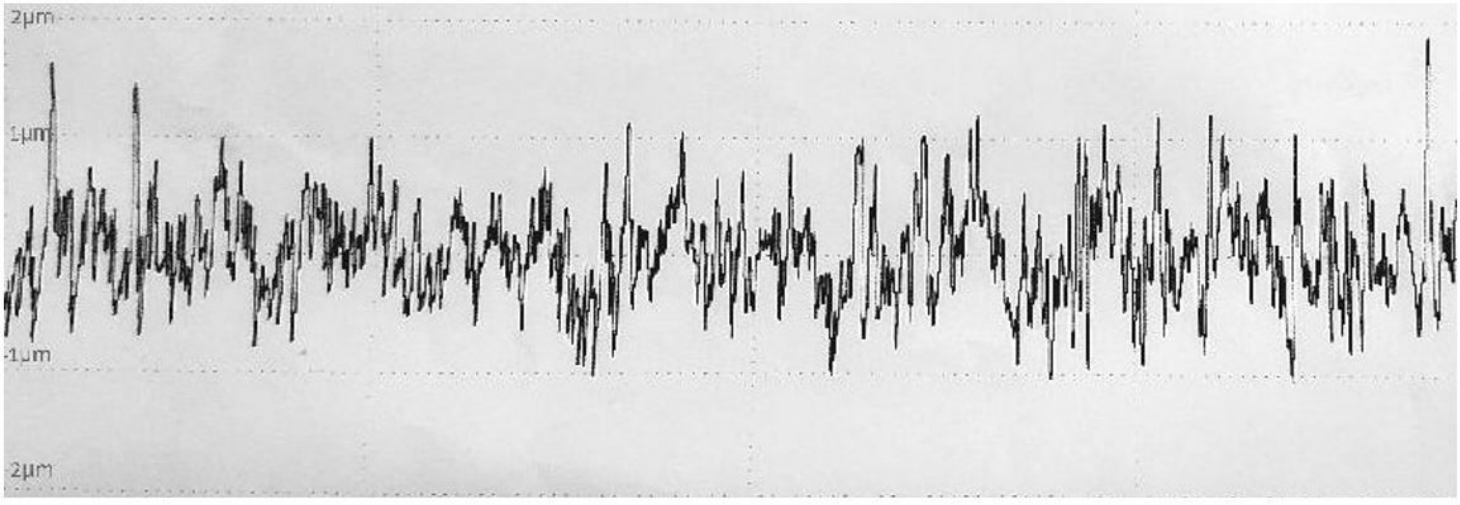

Figure 4

Surface Roughness profile, coolant without cleaning, cutoff 0.8 mm

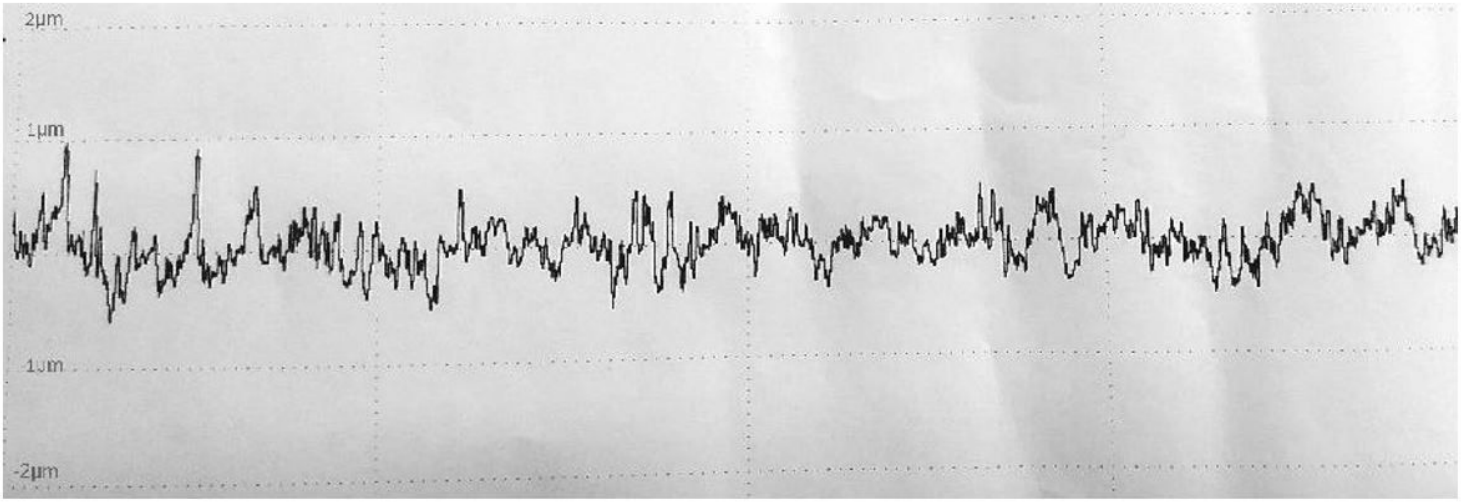

Figure 5

Surface Roughness profile, coolant with cleaning 0°, cutoff 0.8 mm

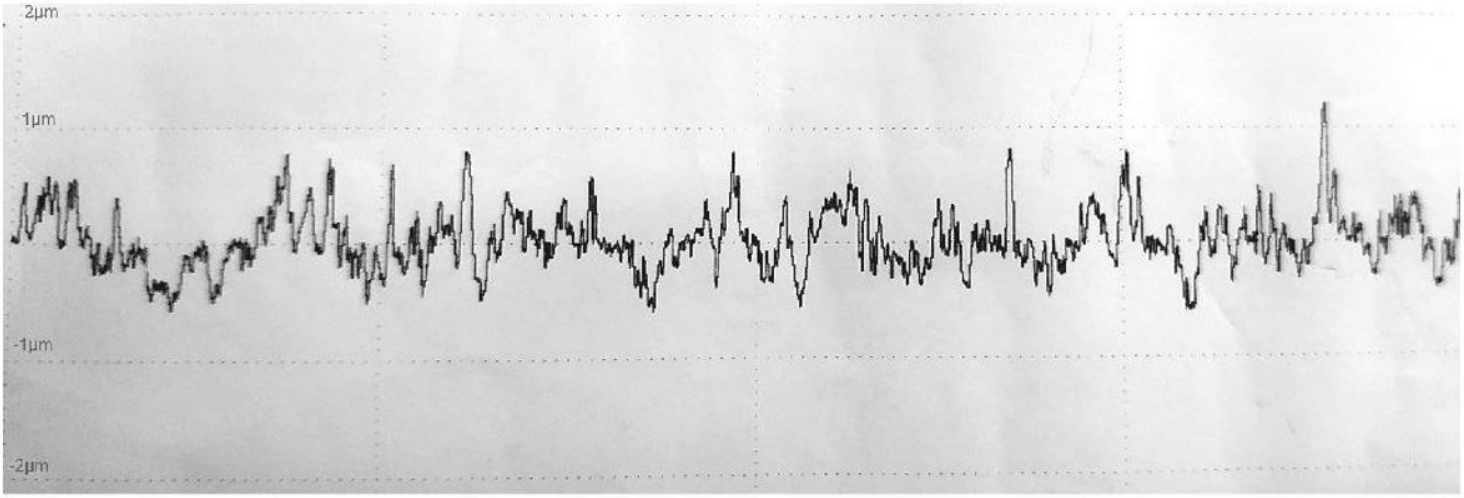

Figure 6

Surface Roughness profile, coolant with cleaning 30°, cutoff 0.8 mm

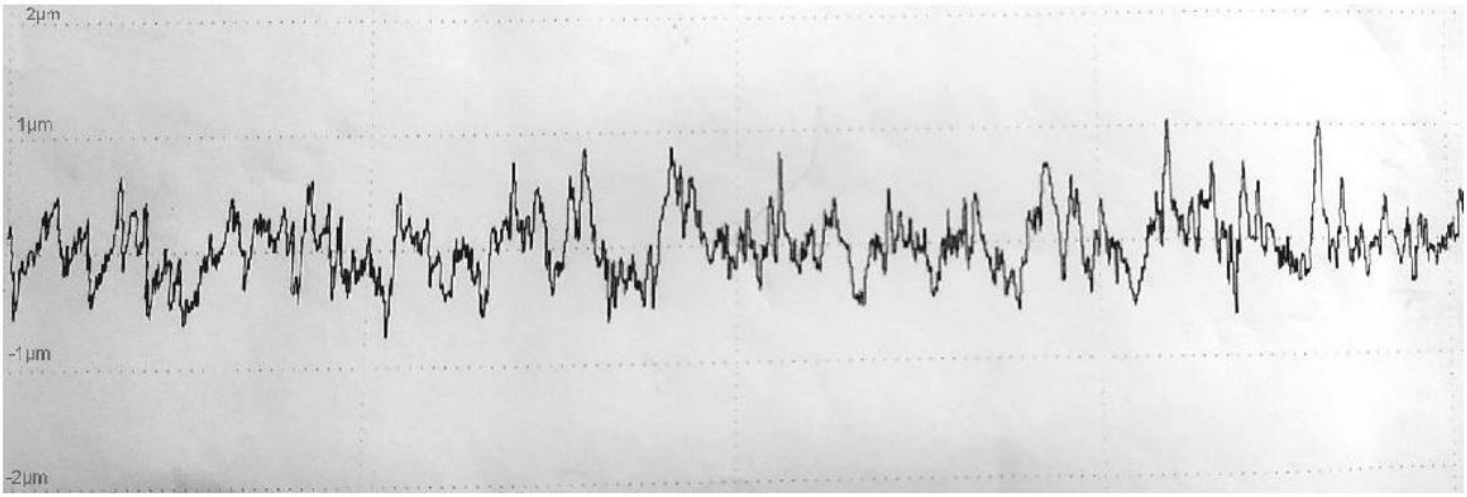

Figure 7

Surface Roughness profile, coolant with cleaning 45°, cutoff 0.8 mm

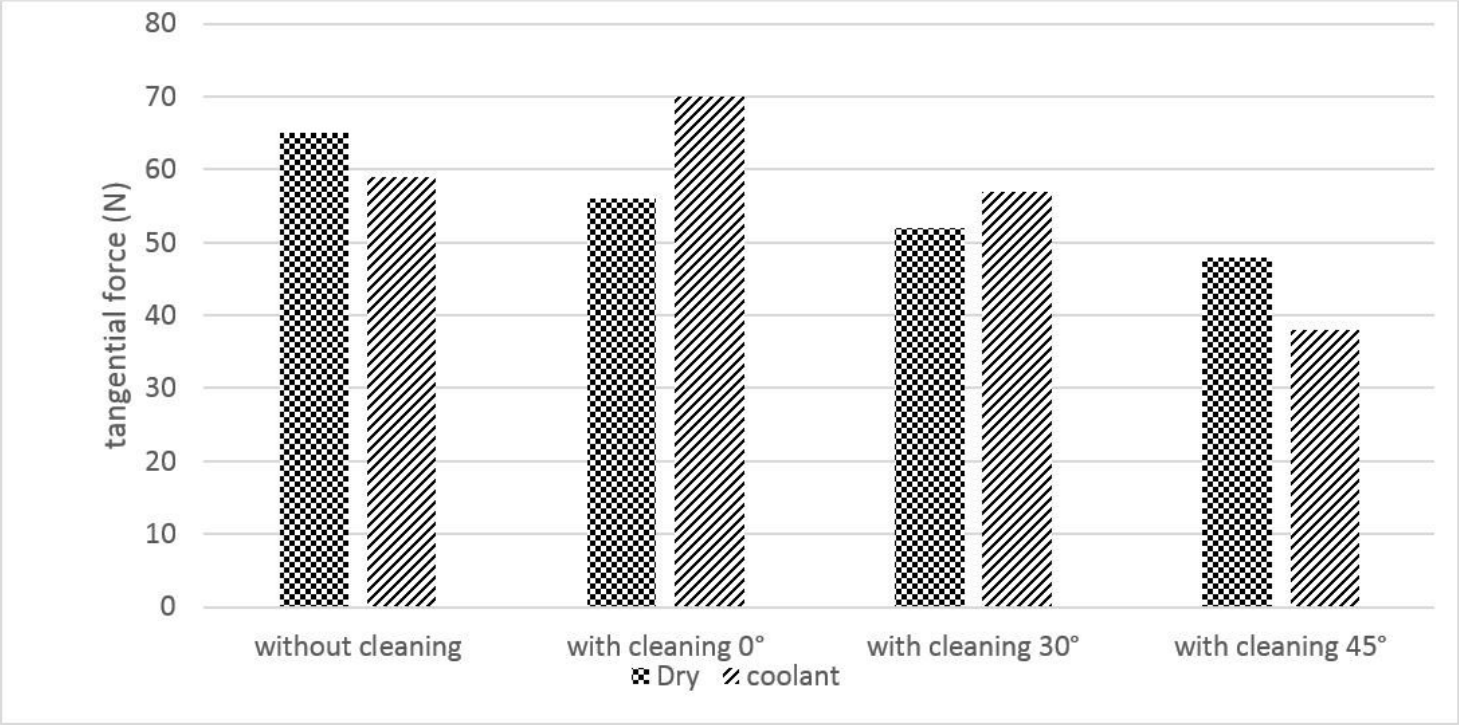

Figure 8

Tangential grinding force

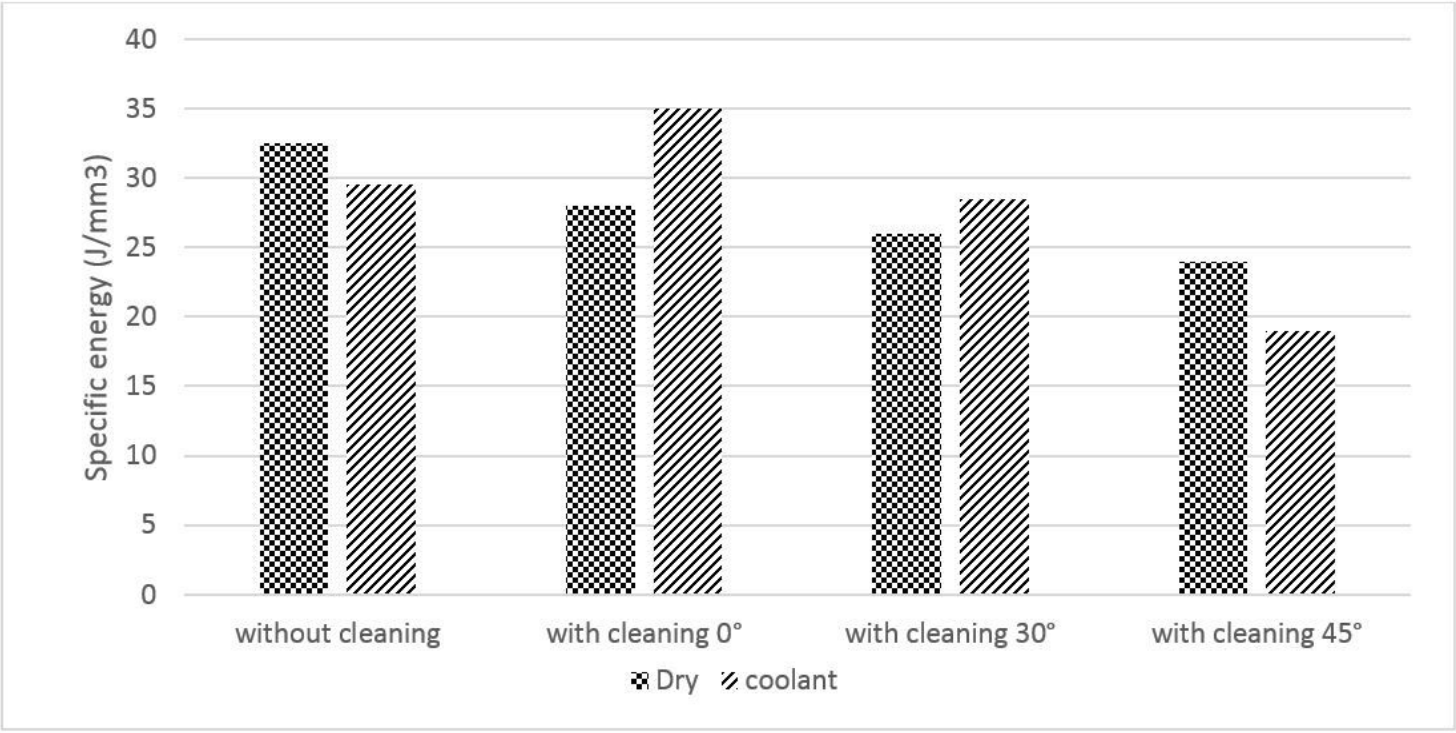

Figure 9

grinding specific energy

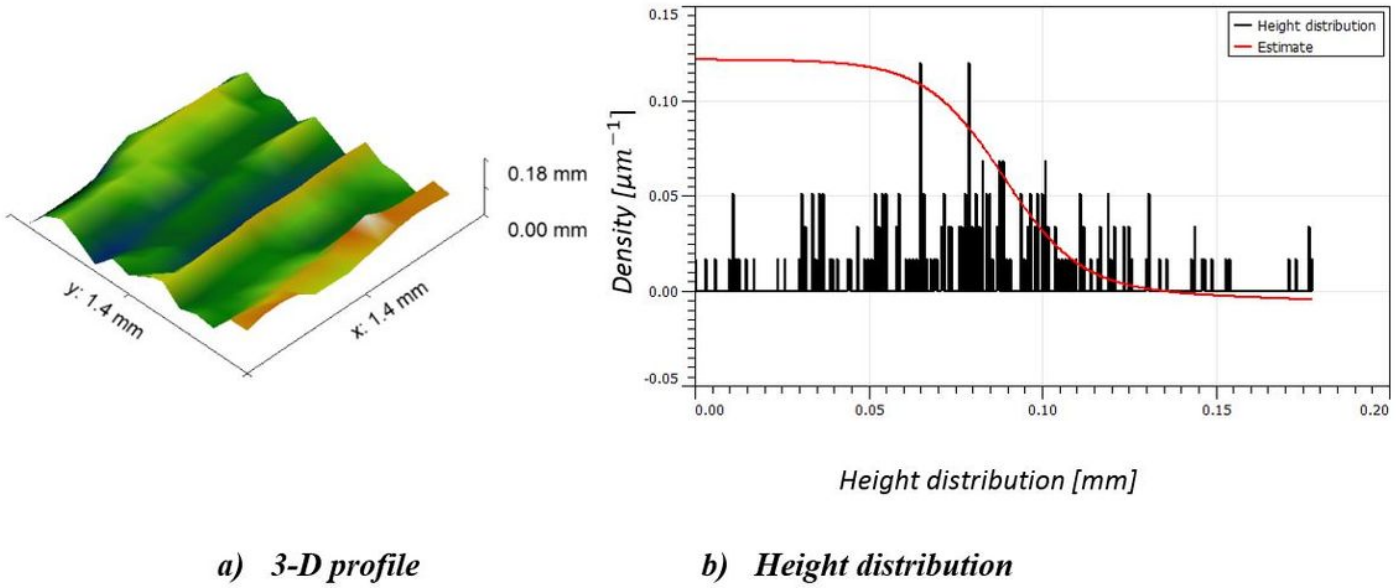

Figure 10

3-D profile and its height distribution at Dry state without cleaning

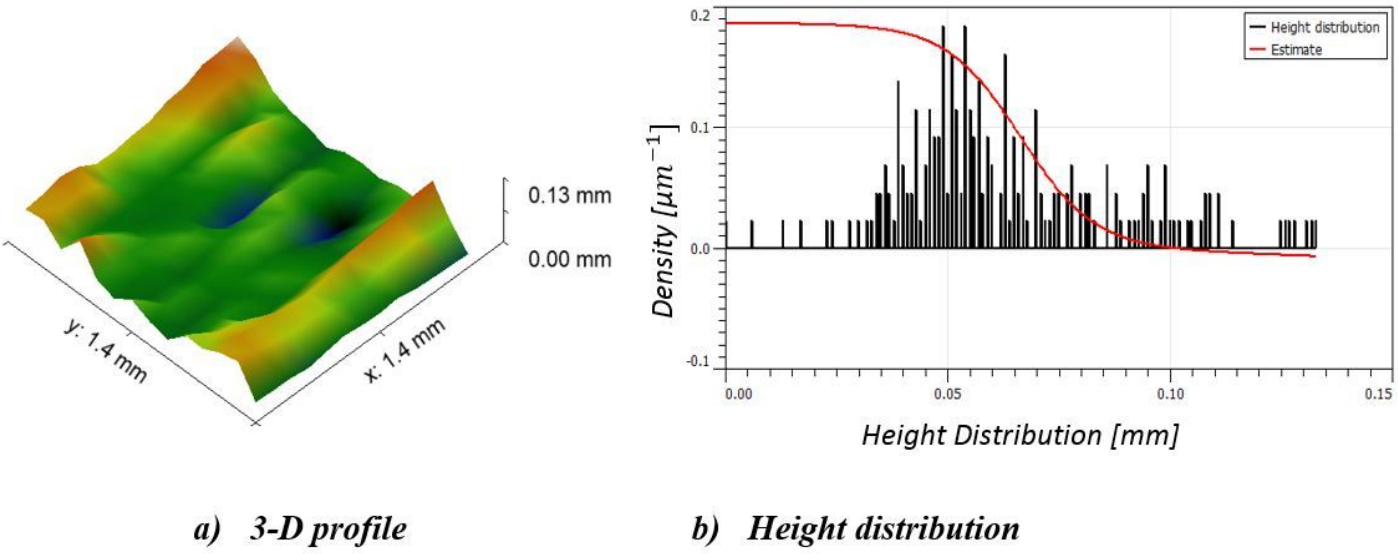

Figure 11

3-D profile and its height distribution at Dry state with cleaning under 45°

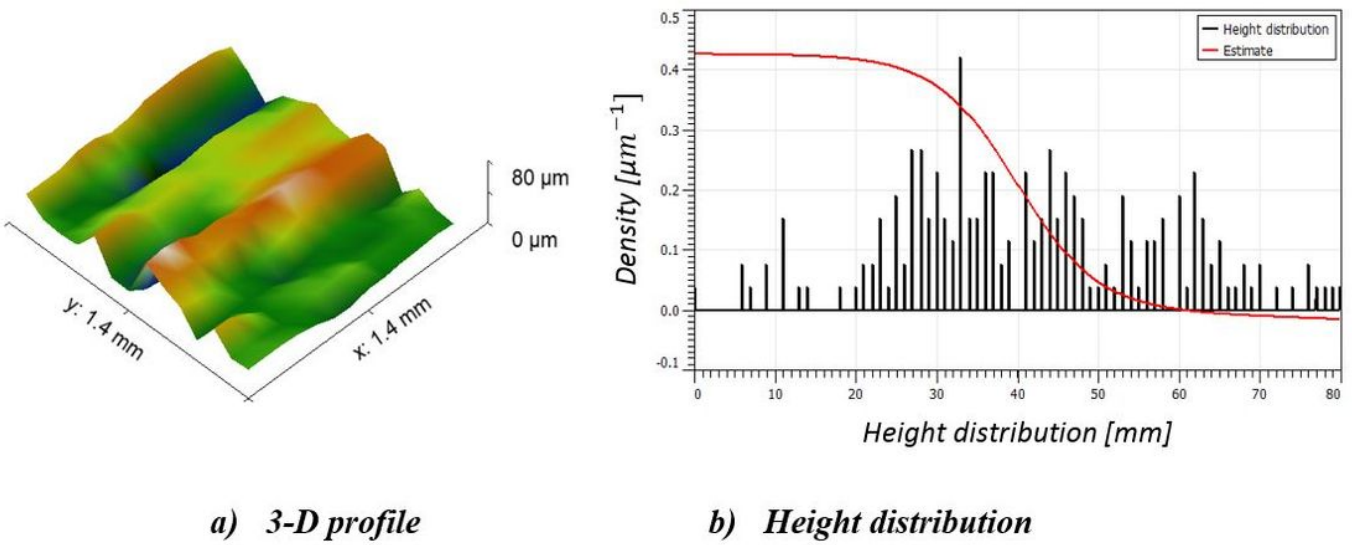

a) 3-D profile *b) Height distribution*

Figure 12

3-D profile and its height distribution at coolant state without cleaning

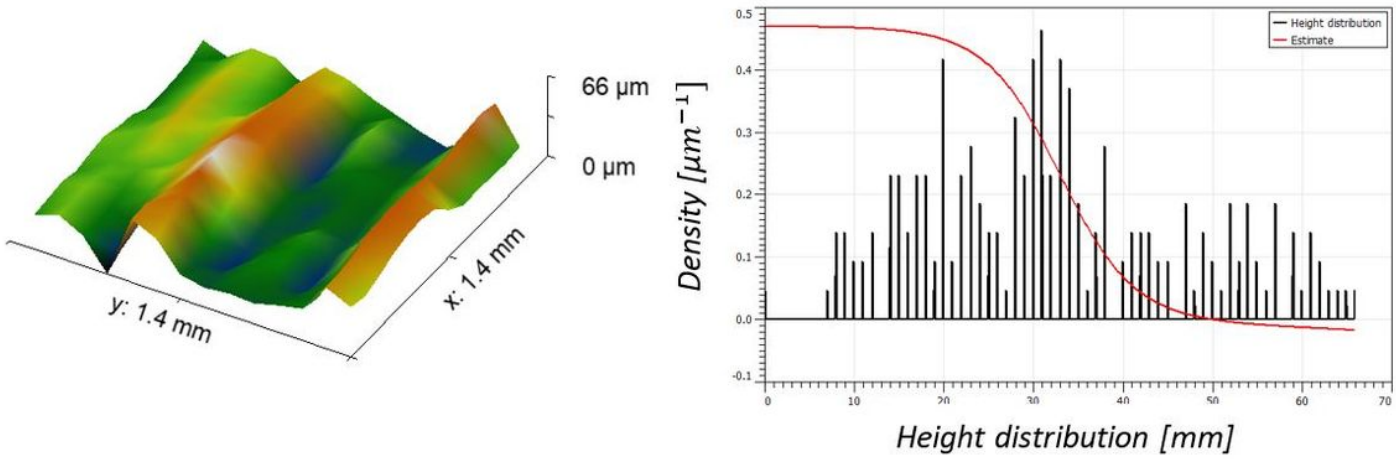

a) 3-D profile *b) Height distribution*

Figure 13

3-D profile and its height distribution at coolant state with cleaning under 45°

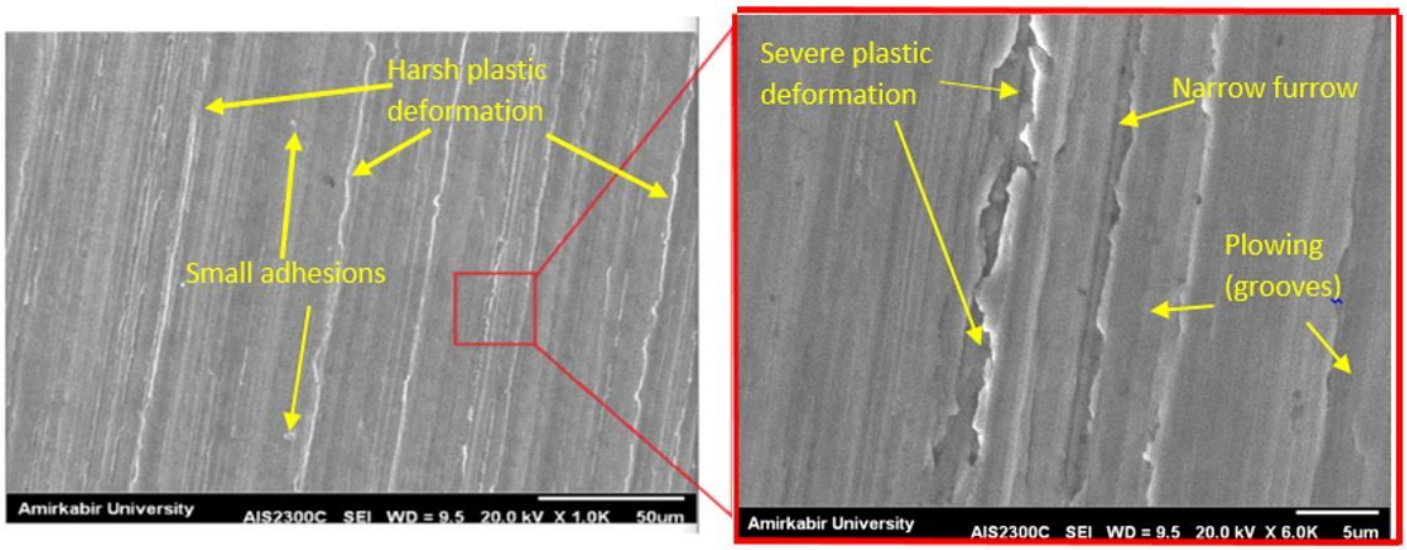

a) SEM image with 1000x magnification *b) SEM image with 6000x magnification*

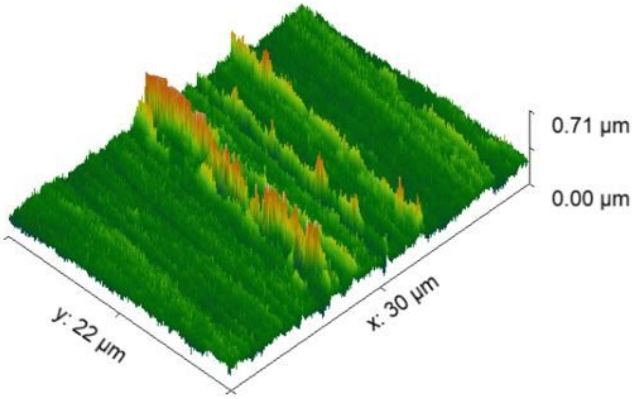

c) 3-D profile

Figure 14

Images of ground surface under dry state using cleaning nozzle at 45°

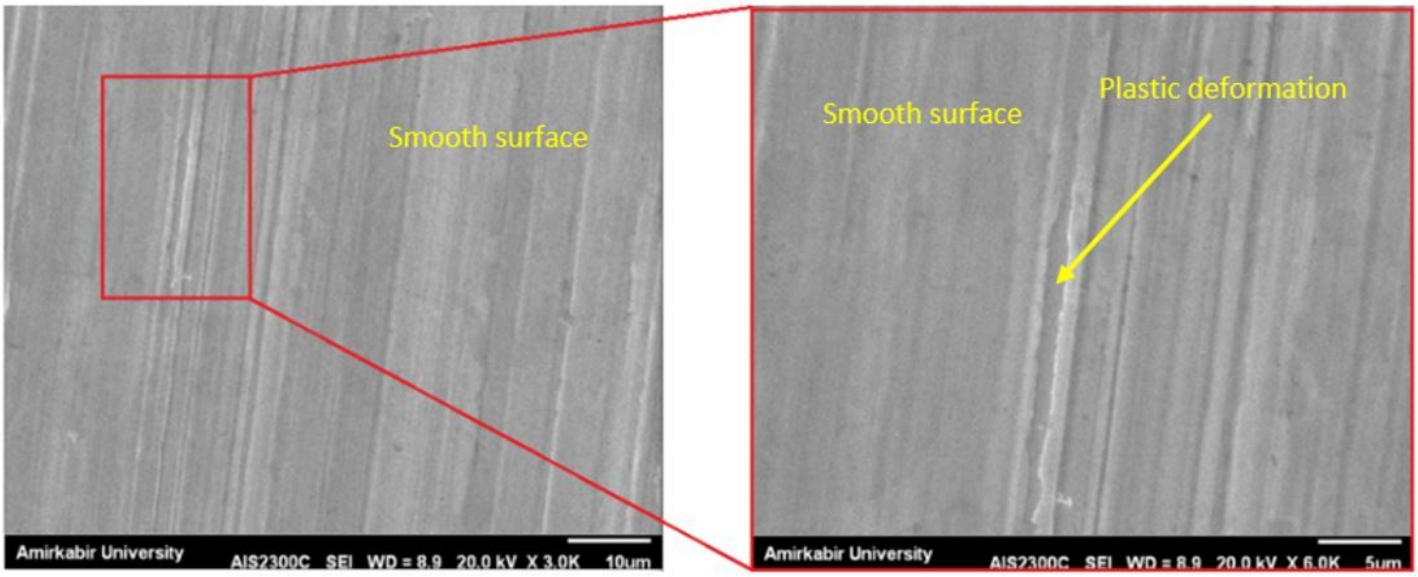

a) SEM image with 3000x magnification *b) SEM image with 6000x magnification*

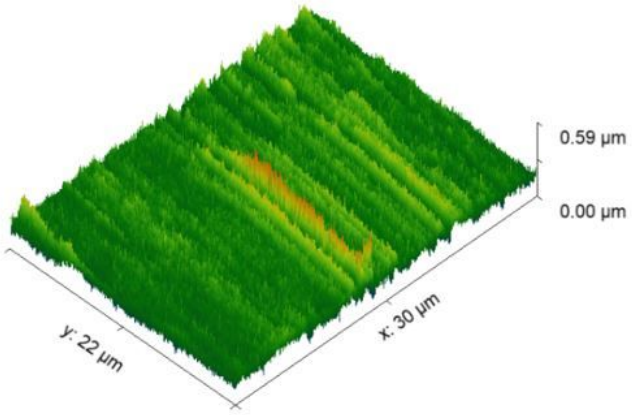

c) 3-D profile

Figure 15

Images of ground surface under Coolant state using cleaning nozzle at 45°

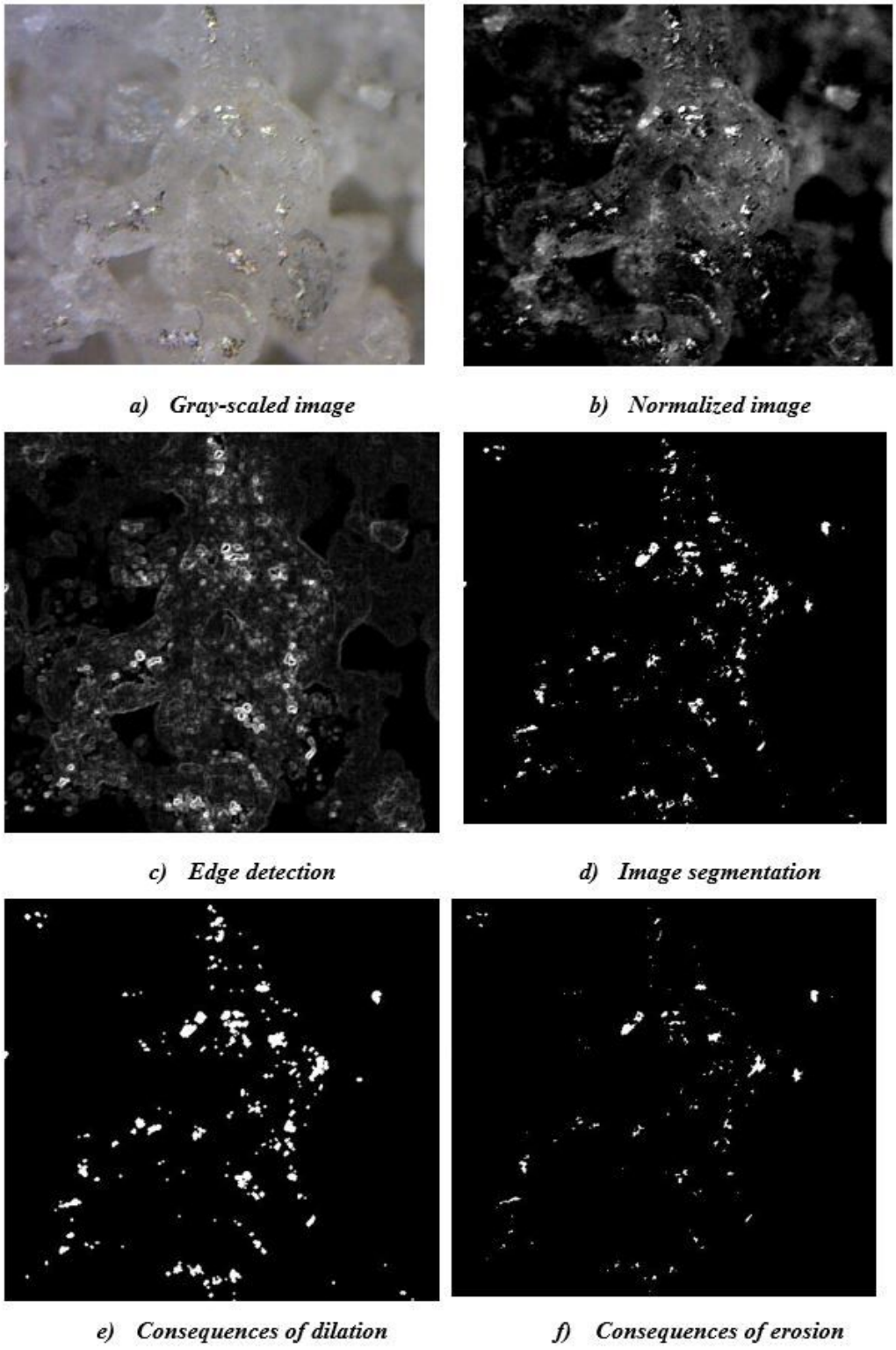

Figure 16

image processing techniques in detecting wheel loading

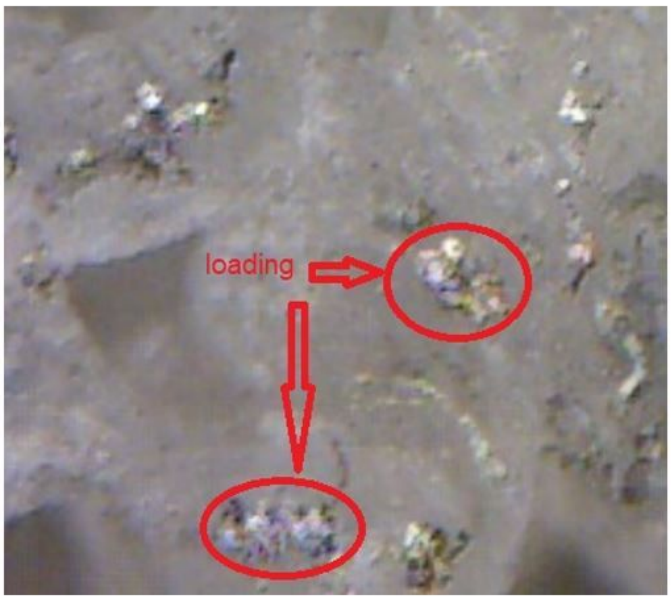

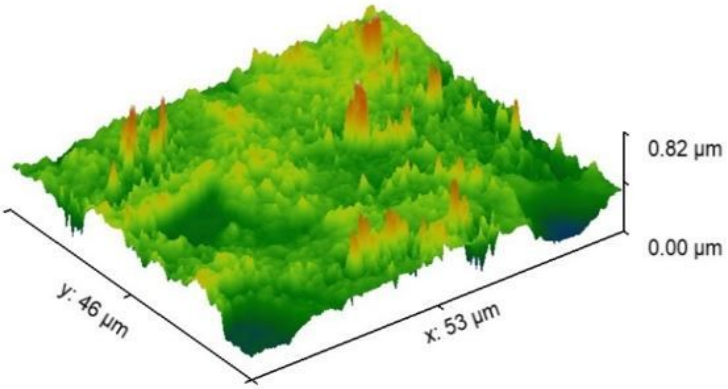

a) Topography of wheel surface *b) 3-D surface profile*

Figure 17

wheel surface

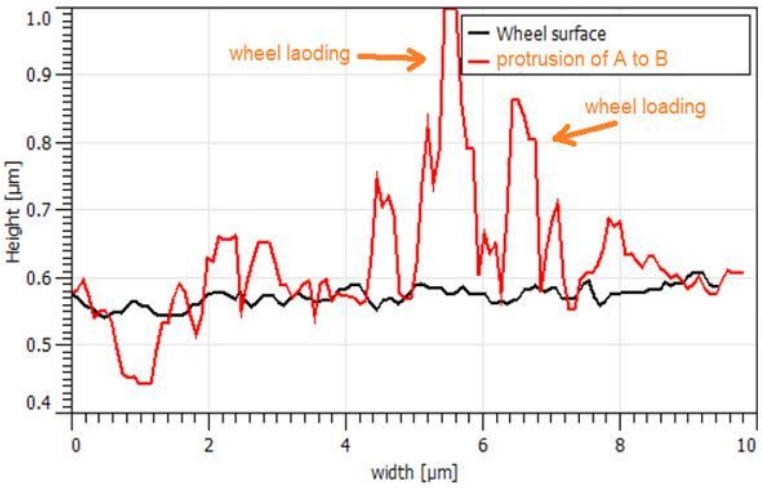

a) chips clogged on wheel surface *b) protrusion of A to B*

Figure 18

protrusion of clogged chips on wheel surface

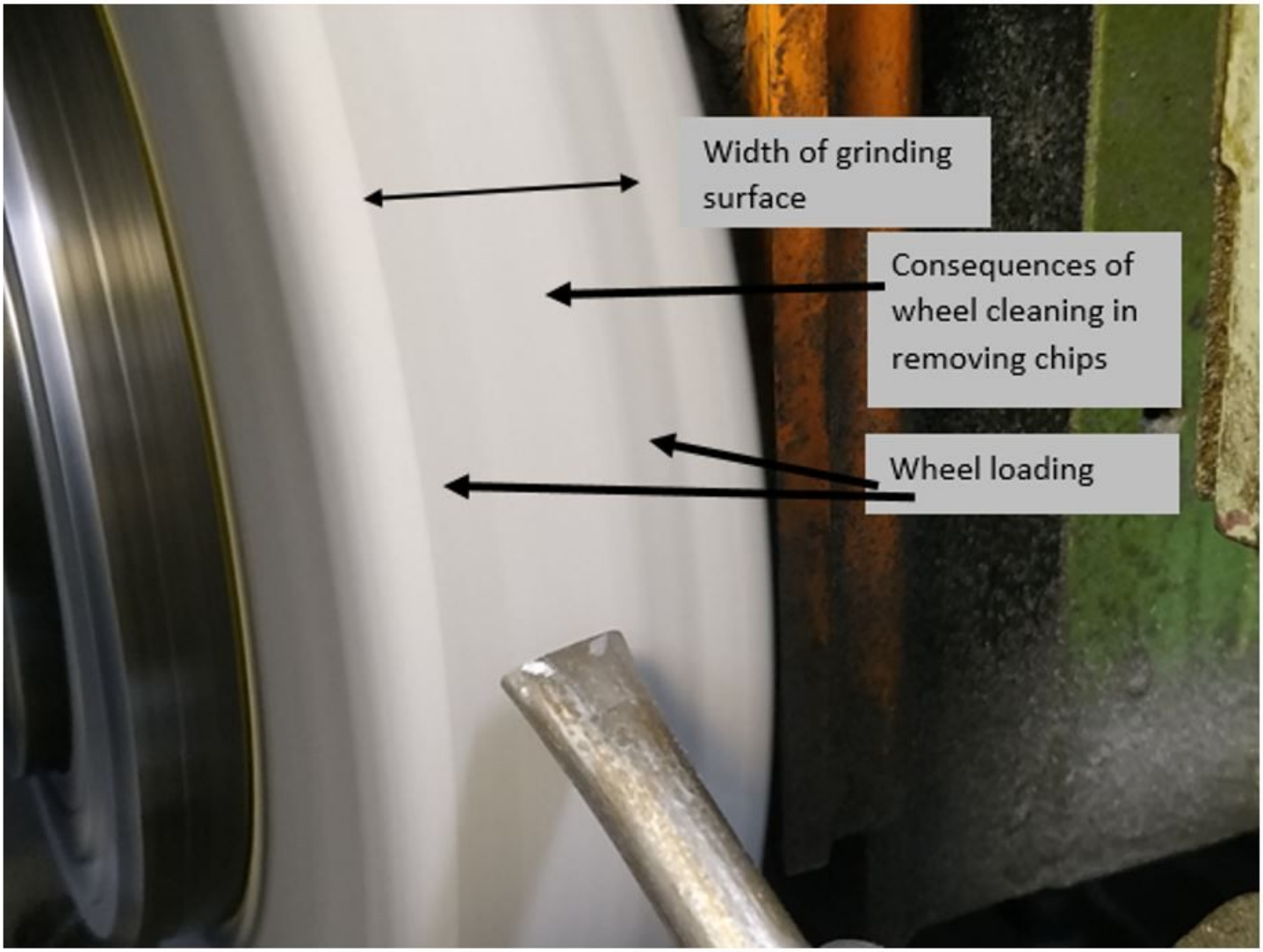

Figure 19

wheel surface cleaning under the incident angle of 45°

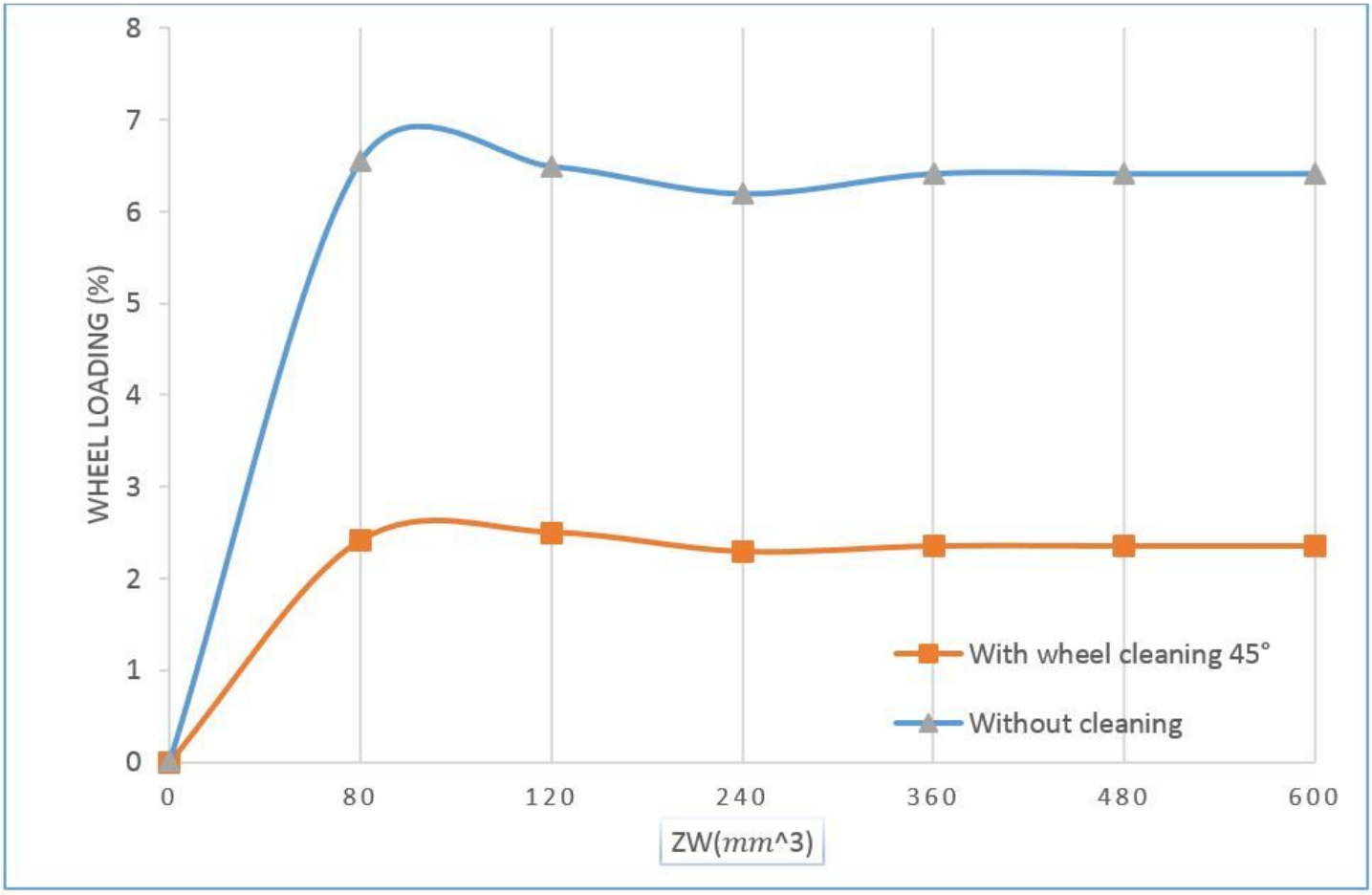

Figure 20

wheel loading over volumetric material removal in Dry state.

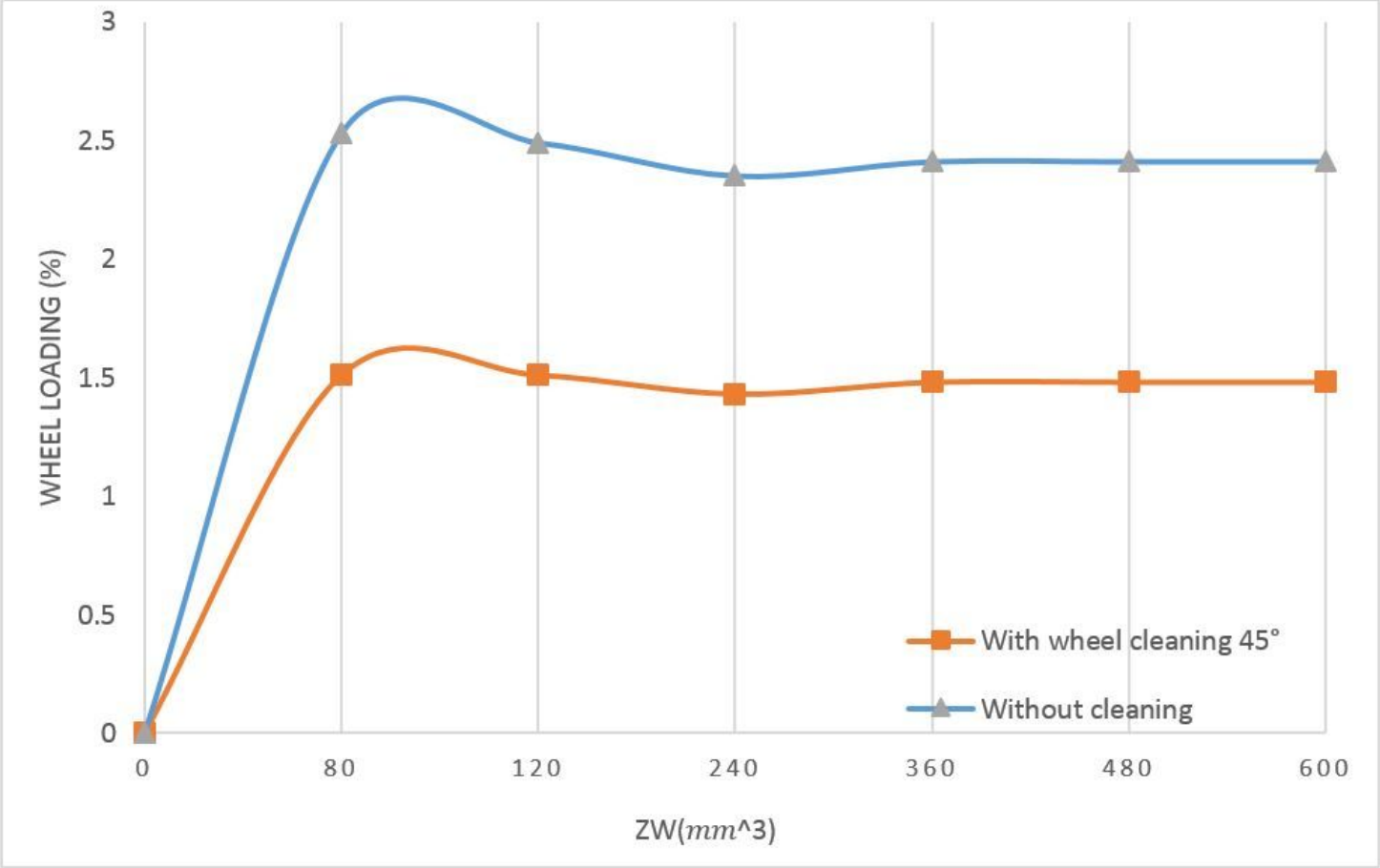

Figure 21

wheel loading over volumetric material removal in coolant state.

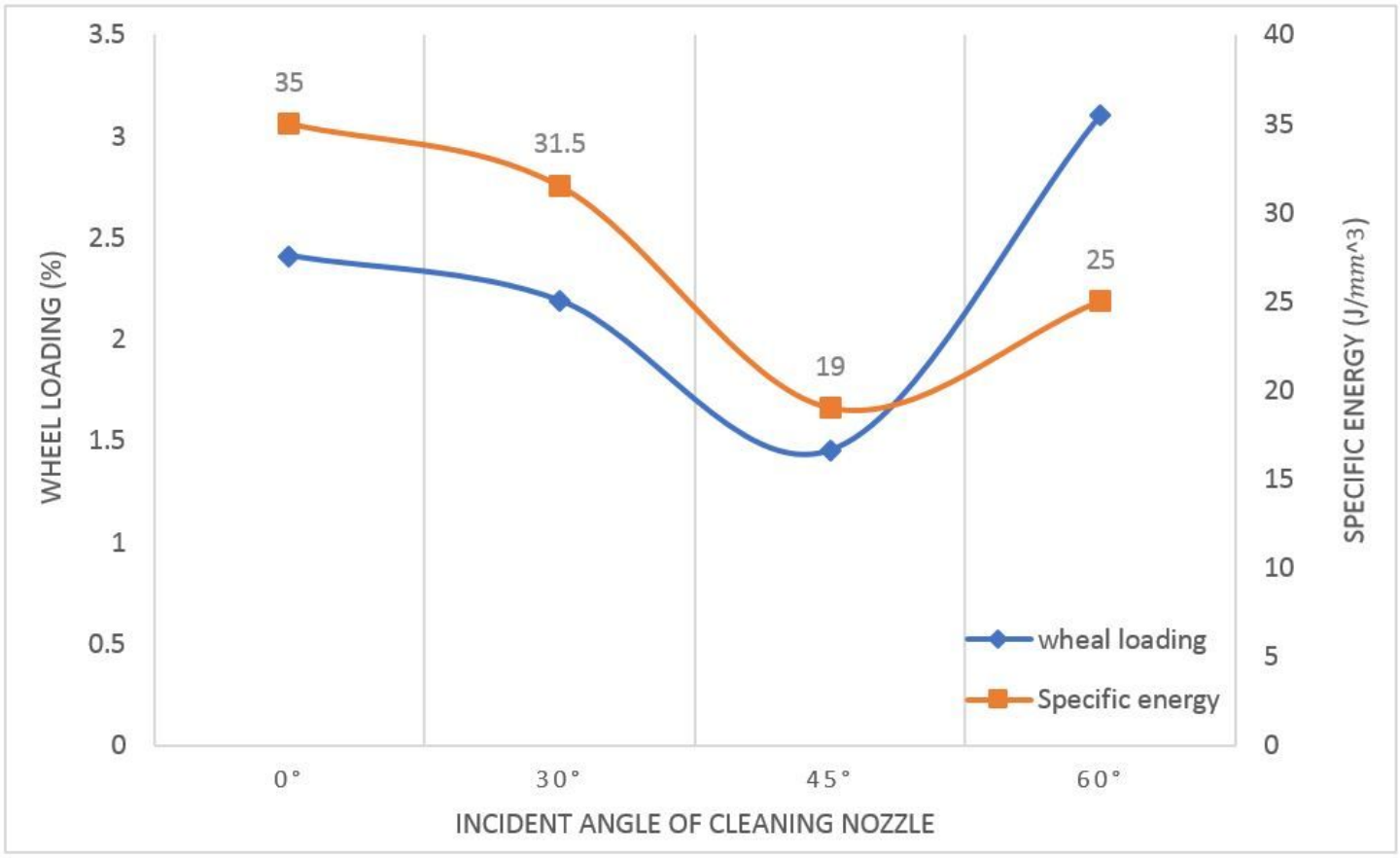

Figure 22

wheel loading and specific energy in different incident angle over volumetric material removal

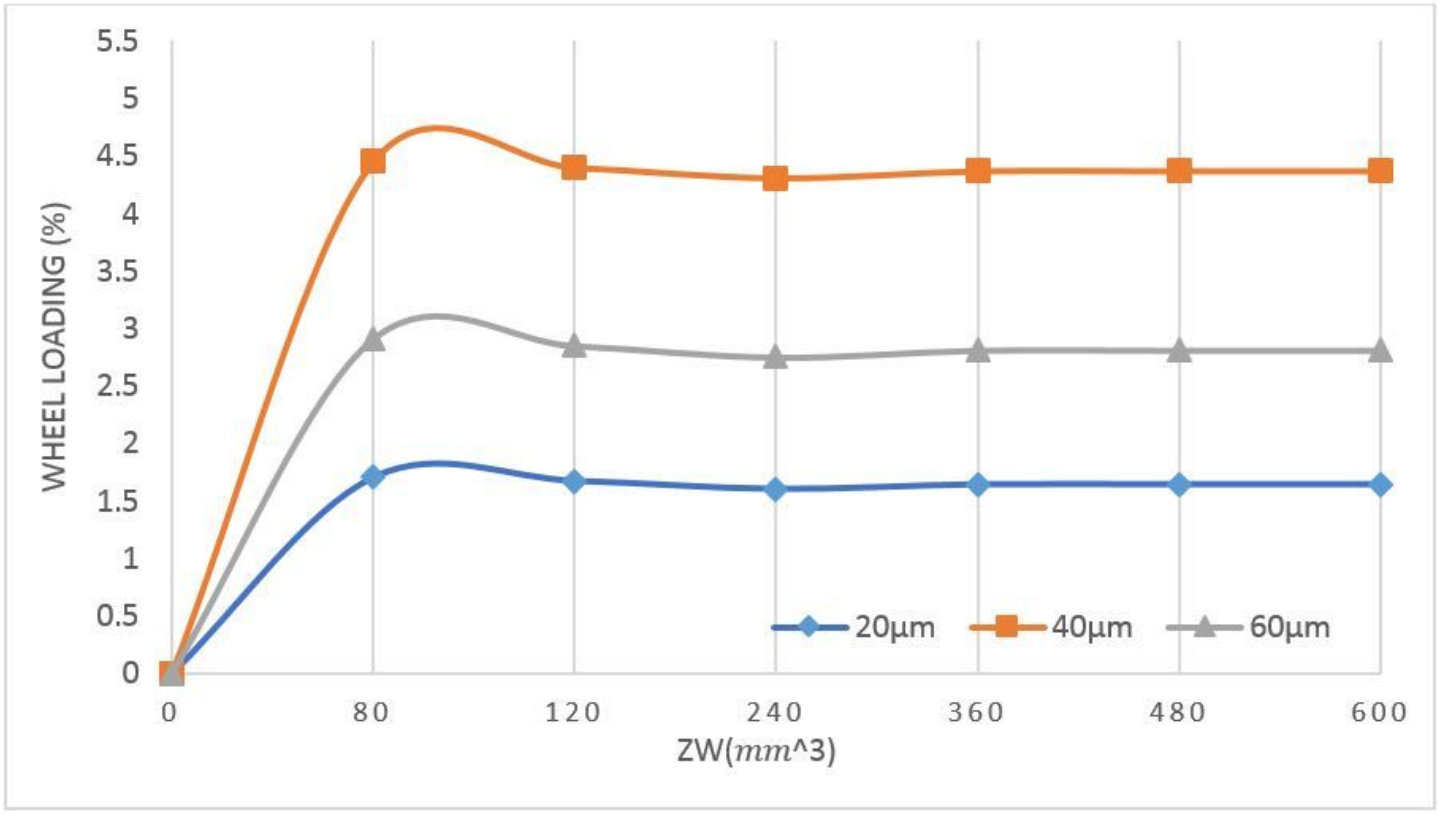

Figure 23

Wheel loading against volumetric material removal with changes in depth of cut.

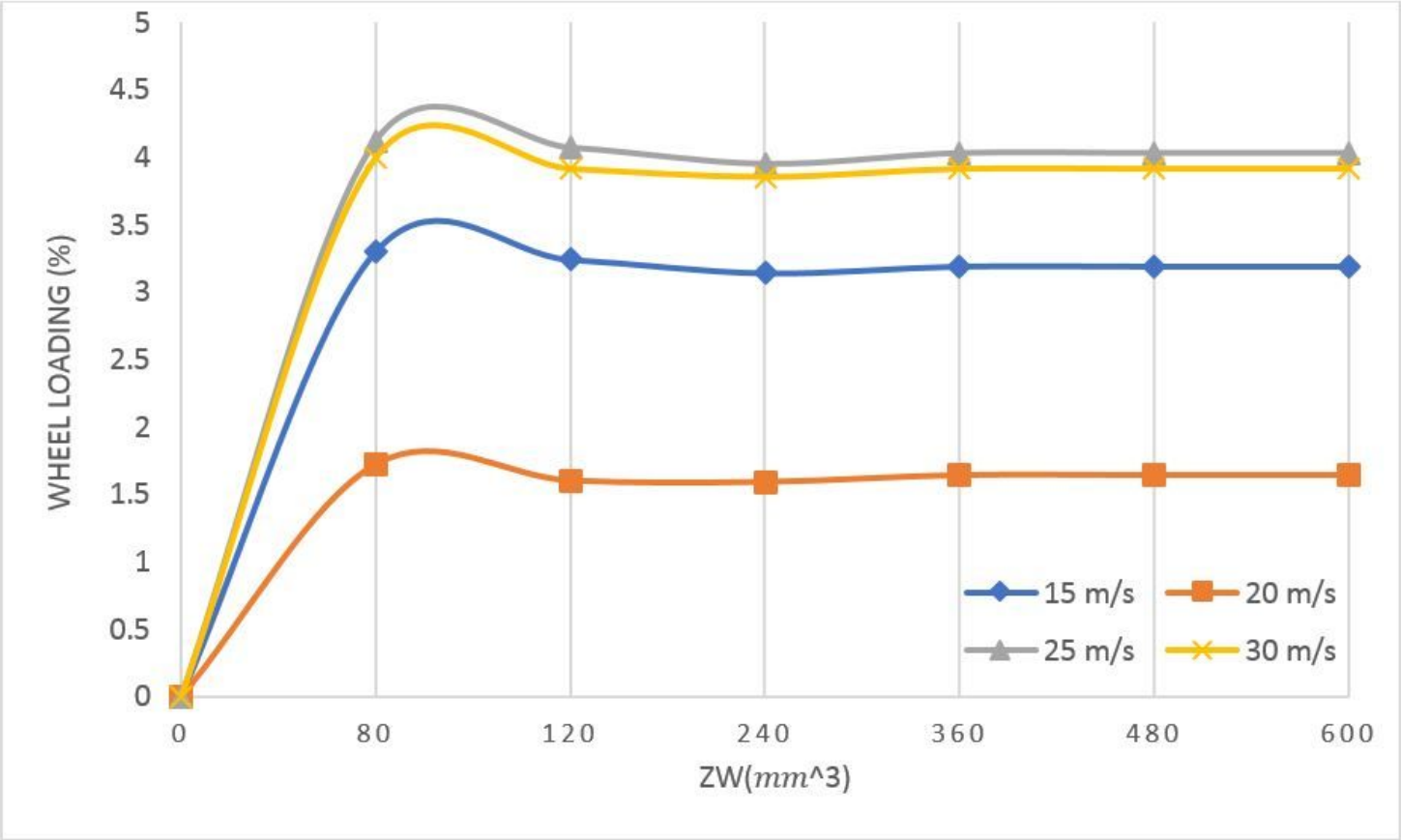

Figure 24

Wheel loading against volumetric material removal with changes in cutting speed.

Supplementary Files

This is a list of supplementary files associated with this preprint. Click to download.

- Graphicalabstract.docx